GPS/GLONASS Combined Precise Point Positioning With the Modeling of Highly Stable Receiver Clock in the Application of Monitoring Active Seismic Deformation

X. Chen[1], C. Lu[1] (ID), B. Guo[2], F. Guo[3,4], M. Ge[1], X. Li[1] (ID), and H. Schuh[1] (ID)

[1]German Research Centre for Geosciences GFZ, Potsdam, Germany, [2]The First Monitoring and Application Center, China Earthquake Administration, Tianjin, China, [3]Collaborative Innovation Center for Geospatial Technology, Wuhan, China, [4]School of Geodesy and Geomatics, Wuhan University, Wuhan, China

Abstract The high-rate kinematic Precise Point Positioning (PPP) of the Global Navigation Satellite System has become an effective method for monitoring crustal deformation caused by earthquakes. In this contribution, the method of GPS/GLONASS PPP with the receiver clock modeling is applied in active seismic deformation monitoring for the first time. With the modeling method, the short-term vertical positioning accuracy of 2–4 mm that usually cannot be obtained by standard PPP is achieved. Our PPP results confirm that the positioning accuracy is improved due to the increase of GLONASS observations compared to the GPS-only solution. Based on the external seismic data and the high-rate GPS/GLONASS data for the 2011 Japan earthquake and 2010 and 2015 Chile earthquakes, comparative analyses concerning receiver clock modeling are carried out. The results show that a high degree of decorrelation between the height position estimates and receiver clock offsets can be obtained by using the receiver clock modeling. The short-term accuracy of the GPS-based vertical displacements is improved to the level of about 4.4 mm, and the short-term accuracy of better than 4 mm for the GPS/GLONASS-combined vertical displacements is achievable. Furthermore, the weak vertical signals that are not detected by standard PPP can be captured with the modeling of highly stable receiver clock.

1. Introduction

For the purpose of rapid and accurate inversion of geophysical parameters of seismic events, it is ultimately necessary to obtain both earthquake-induced static and dynamic displacements as faithfully as possible. Traditionally, seismic displacements are acquired by integration of accelerometer signals or velocities observed with broadband seismometers. However, the two instruments are either easily saturated or clipped, especially for large earthquakes ($M > 7$) and thus can produce completely unrealistic displacements (Boore et al., 2002). In order to avoid the uncertainties, the potential of GPS seismology was first pointed out by Hirahara et al. (1994), focusing on short baselines. Afterward, more studies have demonstrated the capability of GNSS (Global Navigation Satellite System) for monitoring seismic displacement. PPP, as one of GNSS precise positioning techniques, allows for the determination of absolute positions with stand-alone GNSS receivers and is being successfully applied in geodynamics, geodesy, and seismology (Ge et al., 2000; Kouba, 2003; Larson, 2009). In the standard PPP solution, the International GNSS Service (IGS) precise orbit and clock products can be used for correcting the satellite clock biases, while the receiver clock biases are usually introduced as an additional parameter and modeled as white noise at each observation epoch (Cai & Gao, 2013; Ge et al., 2008; Li et al., 2013; Li, Ge, et al., 2015; Li, Zhang, et al., 2015; Zhang & Andersen, 2006). Although this method applies well for low-quality receiver clocks (e.g., quartz crystal oscillators), the intrinsic characteristics of a stable clock over a short interval are inevitably neglected in the case that the highly stable oscillators are connected to the GNSS receivers.

Currently, there are several continuously operating IGS stations equipped with oscillators of H-maser frequency standard (URL: ftp://ftp.igs.org/pub/station/general/loghist.txt), which provides a great potential for carrying out the investigations on receiver clock modeling and its scientific applications. The modeling for highly stable GNSS receiver clocks has been involved in several studies. The feasibility studies of receiver clock modeling in GPS-only precise data processing were first performed by Weinbach and Schön (2011, 2013). Afterward, Wang and Rothacher (2013) started to investigate both the deterministic model and the

stochastic model for high-stable ground receiver clocks. In GPS-only solution, Weinbach and Schőn (2015) further proposed a piecewise linear parameterization of receiver clocks based on the batch least squares estimation and analyzed the 2010 Chile earthquake through high-rate GPS data. However, all the above mentioned studies on receiver clock modeling are entirely limited to the GPS-only observations and increasing the number of GNSS satellites can enhance the observation geometry and thus improve the precise positioning accuracy (Wang et al., 2015). Thus, GPS/GLONASS combined PPP with the receiver clock modeling is used for seismic displacement monitoring in this study.

In the case of standard PPP, the receiver clock offset parameters are modeled as white noise and estimated at every epoch without considering its potential short-term temporal correlation. The vertical positioning accuracy is degraded in the standard PPP solution because of a high correlation between the receiver clock and height estimates (Wang et al., 2015). For PPP-based seismic studies, subtle vertical seismic signals are certainly masked by the huge noise of height estimates. In order to detect these seismic signals, the receiver clock modeling is employed to lower the mathematical correlation between the receiver clock and height estimates and thus improve the accuracy of PPP-derived active seismic waveforms.

The method of GPS/GLONASS PPP with the receiver clock modeling is described in section 2. Then, the frequency stabilities for different receiver clock types are evaluated in terms of the modified Allan deviation in section 3. Using high-rate data prior to the earthquake, we demonstrate that the position accuracy of kinematic PPP (KPPP) with the receiver clock modeling can be improved by adding extra GLONASS observations in section 4. In section 5, the impact of the receiver clock modeling on seismic displacement monitoring is investigated based on the data of the 2011 Japan earthquake and the Chile earthquakes in 2010 and 2015. Finally, we present the conclusions and summaries in section 6.

2. GPS/GLONASS PPP With the Modeling of Receiver Clock

As satellite navigation systems (e.g., GPS, Galileo, QZSS, GLONASS, and BDS) are developing rapidly, the fusion of GNSS further enhances the positioning reliability and accuracy. The GNSS systems are referred to as GPS and GLONASS in this study. The Chinese BDS system is expected to be applied into this field once it supports global navigation and positioning services in 2020. Currently, the Galileo system has 15 satellites in orbits including In Orbit Validation (IOV) and Full Operational Capability (FOC) satellites available for global services. Japan's QZSS system has already supported the positioning services for the East Asia area. Meanwhile, more continuously operating IGS sites are equipped with highly stable atomic receiver clocks, which can provide a good opportunity to investigate receiver clock modeling in KPPP. In the following, we will introduce the relevant observation equations and the receiver clock modeling method for GPS/GLONASS combined PPP, respectively.

2.1. Observation Equation

Considering the receiver clock modeling and timescale differences, the ionosphere-free (IF) observation equations for PPP are expressed as formula (1):

$$
\begin{cases}
P^G = \rho^G + c\left(\delta t_r + \Delta t \cdot \delta t_r{}'\right) - c\delta t_s^G + m_{\text{trop}}^G \cdot \delta_{\text{zwd}} + \varepsilon_P^G \\
L^G = \rho^G + c\left(\delta t_r + \Delta t \cdot \delta t_r{}'\right) - c\delta t_s^G + m_{\text{trop}}^G \cdot \delta_{\text{zwd}} + b^G + \varepsilon_L^G \\
P^R = \rho^R + c\left(\delta t_r + \Delta t \cdot \delta t_r{}' + \delta t_{\text{sys}}\right) - c\delta t_s^R + m_{\text{trop}}^R \cdot \delta_{\text{zwd}} + \varepsilon_P^R \\
L^R = \rho^R + c\left(\delta t_r + \Delta t \cdot \delta t_r{}' + \delta t_{\text{sys}}\right) - c\delta t_s^R + m_{\text{trop}}^R \cdot \delta_{\text{zwd}} + b^R + \varepsilon_L^R
\end{cases}
\tag{1}
$$

where P and L denote the IF pseudorange and IF carrier phase observations. R and G represent the GLONASS and GPS satellites, respectively. ρ denotes the geometric distance from receiver to satellite. c denotes the speed of light in vacuo. Provided that a highly stable oscillator is relatively stable over the short interval Δt, the characteristics of receiver clocks can be described by a two-state temporal model including one time offset parameter δt_r and one frequency offset parameter $\delta t_r{}'$. δt_{sys} is the inter-system bias (ISB). Using precise clock products provided by the ESA IGS analysis center, satellite clock offsets (namely, δt_s^G and δt_s^R) can be corrected. As for troposphere path delays, we obtain the hydrostatic and wet mapping functions m_{trop} by using hydrostatic and wet VMF1 coefficients from the global pressure and temperature 2 wet (GPT2w) model (Böhm et al., 2015). The residual zenith wet delay (ZWD) estimate δ_{zwd} is modeled as random walk. b is the

float ambiguity. ε includes multipath effects and the measurement noise. The error components such as phase wind-up effect, Earth tides, phase center offsets and variations, ocean tide loading, and relativistic effect are corrected using conventional methods (Kouba & Héroux, 2001).

2.2. Receiver Clock Modeling

The frequency stability of oscillators used by receiver clocks is critical for receiver clock modeling since it directly affects the short-term variations of receiver clock offset over the clock modeling interval. It is possible to degrade the PPP performance with the receiver clock modeling if accumulated errors caused by random frequency fluctuations over the interval exceed the carrier phase observation noise. Therefore, we need to evaluate the frequency stability prior to receiver clock modeling.

As an effective method of evaluating the frequency stability, the modified Allan variance $\text{Mod } \sigma_y^2$ in terms of δt_j can be expressed as equation (2):

$$\text{Mod } \sigma_y^2 = \frac{1}{2n^4\tau_0^2(N-3n+1)} \cdot \sum_{i=1}^{N-3n+1} \left(\sum_{j=i}^{i+n-1} \left(\delta t_{j+2n} - 2\delta t_{j+n} + \delta t_j \right) \right)^2 \tag{2}$$

where N is the number of samples at an interval of τ_0, δt_j represents the clock offset, and n is the smoothing factor, ranging from 1 to $\text{int}\{(N^{-1})/2\}$. Based on zero baseline results, Weinbach compared the modified Allan variance with the standard overlapping Allan variance and demonstrated that the modified Allan variance was more sensitive to distinguish between white and flicker frequency noises (Weinbach, 2013). Thus, the modified Allan variance is employed to evaluate the frequency stability of receiver clock in this study.

For a specific highly stable receiver clock, we should select an appropriate model and introduce relative constraints into PPP over a given time period, provided that the frequency stability meets the requirement for receiver clock modeling. Considering the strong temporal correlation for highly stable receiver clock offsets, a two-state model consisting of the receiver clock time and frequency offsets is used here.

In this study, the Kalman filter is employed as an estimator for the KPPP solutions. Within the Kalman filter, the state vector is used for describing the dynamic process of PPP. By using the estimated states from the previous time step, we can derive the predicted estimates for the current epoch. The linear system for KPPP can be expressed as follows:

$$\begin{cases} O_p = H_p X_p + \kappa_p \\ X_p = \Phi_{p,p-1} X_{p-1} + T_{p-1} W_{p-1} \end{cases} \tag{3}$$

where p and p-1 denote the current and previous epoch, respectively, O_p is the measurement vector, which is derived from formula (1), H_p is the design matrix for GPS/GLONASS observations, T_{p-1} is the noise drive matrix, $\Phi_{p,p-1}$ denotes the state transition matrix, and κ_p and W_p, respectively, represent the measurement noise and process noise vector, which are assumed as white noise with zero mean and covariance R_p and Q_p; the state vector X_p including five types of estimated parameters (i.e., position, receiver clock time and frequency offsets, ISB, ZWD, GPS, and GLONASS ambiguities) is shown as formula (4):

$$X = \left(x, y, z, \delta t_r, \delta t_r{}', \delta t_{\text{sys}}, \delta_{\text{zwd}}, b_1^G \dots b_n^G, b_m^R \dots b_m^R \right)^T \tag{4}$$

Subsequently, the recursive calculation of the Kalman filter is carried out in order to update the unknown parameters for the current epoch in the kinematic PPP, shown as formulas (5)–(9).

$$\widetilde{X}_{p,p-1} = \Phi_{p,p-1} \cdot X_{p-1} \tag{5}$$

$$P_{p,p-1} = \Phi_{p,p-1} P_{p-1} \Phi_{p,p-1}^T + T_{p-1} Q_{p-1} T_{p-1}^T \tag{6}$$

$$M_p = P_{p,p-1} H_p^T \left(H_p P_{p,p-1} H_p^T + R_p \right)^{-1} \tag{7}$$

$$X_p = \widetilde{X}_{p,p-1} + M_p \left(O_p - H_p \widetilde{X}_{p,p-1} \right) \tag{8}$$

$$P_p = \left(I - M_p H_p \right) P_{p,p-1} \left(I - M_p H_p \right)^T + M_p R_p M_p^T \tag{9}$$

where X_p and P_p are the updated state vector and its covariance matrix, respectively, $\widetilde{X}_{p,p-1}$ and $P_{p,p-1}$ are the
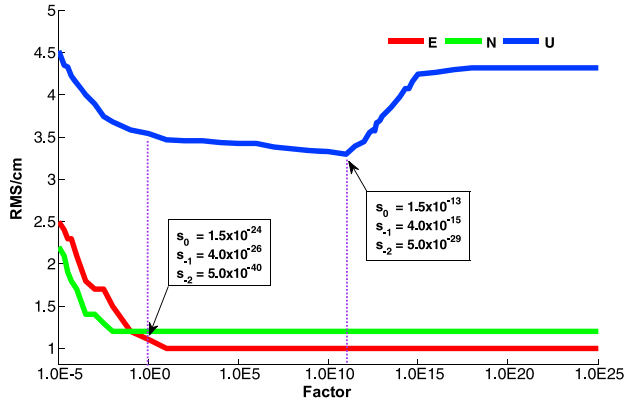
Figure 1. Averaged RMS values of positioning errors in the north, east, and up components at station MGUE for GPS/GLONASS combined kinematic PPP solutions with receiver clock modeling using different multiplying factors of the spectral density coefficients over a period from 1 January 2015 to 1 September 2015.

predicted state vector and its covariance matrix, respectively, M_p represents the filter gain matrix, and I is an identity matrix.

In Kalman filter, the process noise covariance matrix Q_p should be well controlled since the matrix will directly affect the relative epoch-wise constraints on receiver clock offsets. Actually, the receiver clock modeling, as a random ramp approach, is carried out in the process noise covariance matrix with respect to the predicted state $\widetilde{X}_{p,p-1}$. In the Kalman filter approach, the state transition equations for receiver clock parameters can be taken from formulas (3) and (6) as follows:

$$\begin{bmatrix} \delta t_r \\ \delta t_r' \end{bmatrix}_p = \begin{bmatrix} 1 & \Delta t \\ 0 & 1 \end{bmatrix} \cdot \begin{bmatrix} \delta t_r \\ \delta t_r' \end{bmatrix}_{p-1} + \begin{bmatrix} \omega_r \\ \omega_r' \end{bmatrix} \quad , \quad \hat{\Phi}_{p,p-1} = \begin{bmatrix} 1 & \Delta t \\ 0 & 1 \end{bmatrix} \quad (10)$$

$$\hat{P}_{p,p-1} = \hat{\Phi}_{p,p-1}\hat{P}_{p-1}\hat{\Phi}_{p,p-1}^T + \hat{T}_{p-1}\hat{Q}_{p-1}\hat{T}_{p-1}^T$$

$$= \hat{\Phi}_{p,p-1}\hat{P}_{p-1}\hat{\Phi}_{p,p-1}^T + \hat{Q}_{p,p-1} \quad (11)$$

where p is the epoch number, ω_r, ω_r' are process noises, $\hat{P}_{p-1}$ and $\hat{Q}_{p-1}$ are the covariance matrix and the process noise covariance matrix for the estimated receiver clock states at the previous epoch $p-1$, respectively, and $\hat{P}_{p,p-1}$ and $\hat{\Phi}_{p,p-1}$ denote the covariance matrix and the transition matrix for the predicted receiver clock states, respectively. The process noise covariance matrix $\hat{Q}_{p,p-1}$ with respect to the predicted receiver clock states that is essential for receiver clock modeling can be described as formula (12).

$$\hat{Q}_{p,p-1} = \begin{bmatrix} \frac{s_0}{2}\Delta t + 2s_{-1}(\Delta t)^2 + \frac{2}{3}\pi^2 s_{-2}(\Delta t)^3 & \frac{s_0}{2} + 2s_{-1}\Delta t + \frac{2}{3}\pi^2 s_{-2}(\Delta t)^2 \\ \frac{s_0}{2} + 2s_{-1}\Delta t + \frac{2}{3}\pi^2 s_{-2}(\Delta t)^2 & \frac{s_0}{2\Delta t} + 4s_{-1} + \frac{8}{3}\pi^2 s_{-2}\Delta t \end{bmatrix} \quad (12)$$

where s_{-2}, s_{-1}, s_0, represent the spectral power density for the random walk, flicker, and white frequency noises, respectively (Brown & Hwang, 2005; Van Dierendonck et al., 1984). The contribution of the flicker frequency noise that usually cannot be described by a finite-order model is considered in the process noise matrix (Herring et al., 1990; Weinbach, 2013). The original values for $s_{-2}, s_{-1},$ and s_0 are fixed to the typical spectral density coefficients converted from Vremya-CH data (URL: http://www.vremya-ch.com/english/product/). Afterward, we try to adjust the order of magnitude of these coefficients. Based on numerous data analyses of kinematic PPP, the proper spectral density coefficients are obtained for the specific IGS station.

Figure 1 shows the position accuracy in the east, north, and up component at station MGUE for PPP with receiver clock modeling using the different spectral density coefficients. As shown in Figure 1, the position accuracy of PPP with receiver clock modeling is not the best when the typical spectral density coefficients are used. The s_{-2}, s_{-1}, s_0 values for the IGS tracking station MGUE equipped with highly stable H-maser clocks are fixed to $5.0 \times 10^{-29}, 4.0 \times 10^{-15}$, and 1.5×10^{-13} (m²/s), respectively. The empirical values are used in the process noise covariance matrix within Kalman filter in order to add the relative constraints on receiver clock estimates. This is a critical step for receiver clock modeling. In the future, we will further optimize the set of the spectral power density coefficients based on more analyses of kinematic PPP. In addition, all the selected spectral density coefficients involved for this study are listed in Table 1.

Table 1

The Spectral Density Coefficients (Unit: m²/s) for IGS Stations Involved for PPP With Receiver Clock Modeling in the Application of Monitoring Active Seismic Deformation

IGS station	s_0	s_{-1}	s_{-2}
MGUE	1.5×10^{-13}	4.0×10^{-15}	5.0×10^{-29}
SHAO	3.0×10^{-12}	8.0×10^{-14}	1.0×10^{-27}
DAEJ	1.1×10^{-8}	2.1×10^{-9}	0.0
USUD	6.0×10^{-15}	1.6×10^{-16}	2.0×10^{-30}
CONZ	1.2×10^{-17}	3.2×10^{-19}	4.0×10^{-33}

In the PPP processing with receiver clock modeling, we actually adjust the constraints on receiver clock estimates every modeling interval within the Kalman filter. First, a reference clock modeling interval is obtained through the modified Allan deviation test, as described in the following section 3. Afterward, we adjust the reference modeling interval based on numerous data analyses of KPPP and thus select the proper clock modeling interval for a specific IGS station. Over the selected clock modeling interval, a Kalman filter with the random ramp modeling and certain process noise according to $s_{-2}, s_{-1},$ and s_0 coefficients is used. Moreover, the spectral density coefficients should be increased by a factor of 3–5 every modeling interval in
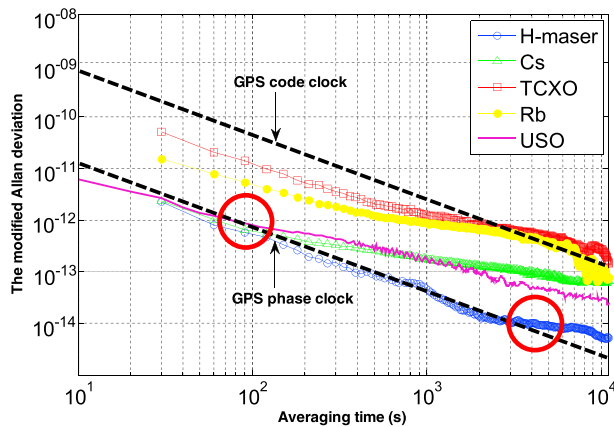
Figure 2. The modified Allan variance for five types of receiver clock offsets from active hydrogen maser (H-maser), ultrastable oscillator (USO), cesium atomic oscillator (Cs), rubidium gas-cell oscillator (Rb), and temperature-compensated quartz crystal oscillator (TCXO), respectively.

order to reduce the accumulated errors for receiver clock estimates that possibly degrade the PPP accuracy.

From the point of view of correlation, the receiver clock modeling undoubtedly causes a change in correlation between each pair of estimates in the PPP solution. For correlation analyses in this study, correlation coefficients are calculated according to equation (13).

$$\rho = \frac{\text{cov}(\delta a, \delta b)}{\sqrt{\sigma_{\delta a}^2 \cdot \sigma_{\delta b}^2}} \tag{13}$$

where ρ represents the correlation coefficient between estimates δa and δb. The covariance $\text{cov}(\delta a, \delta b)$ and variances $\sigma_{\delta a}^2$ and $\sigma_{\delta b}^2$ are obtained from the updated estimate covariance matrix in the Kalman filter, which indicates that the epoch-wise correlation coefficients can be derived for correlation analyses on PPP estimates.

Since the correlation between ISB and other estimates is rather small when sufficient satellites are available for users, the position accuracy of 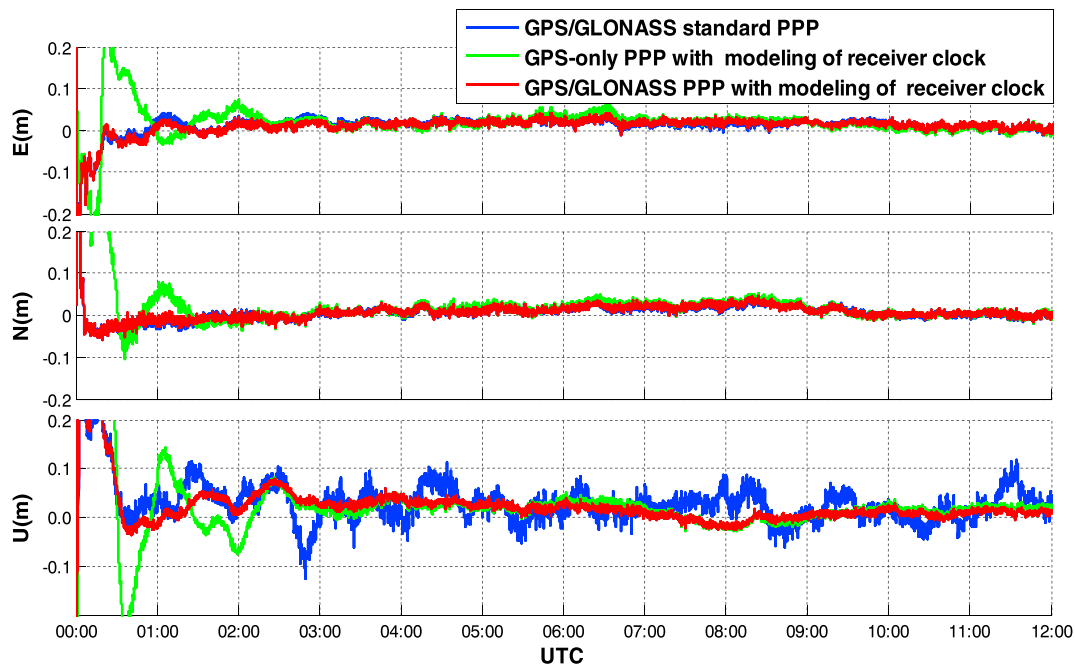GPS/GLONASS combined PPP is slightly impacted by different models of ISB under this condition. As the number of visible satellites decreases, the ISB estimates are more correlated with the position and receiver clock estimates (Wang et al., 2015). For improving the PPP accuracy in the case of poor observational environments, the ISB estimates are modeled as a random walk process in this study.

3. Frequency Stability Analysis of Receiver Clock

Considering the different receiver clock quality, we evaluate and compare the frequency stability for different types of oscillators in use, which is necessary for the subsequent receiver clock modeling.

First, static GPS daily data (with 30-s intervals) on 25 February 2015 of four IGS tracking stations equipped with different types of oscillators are processed using precise clock and orbit products from ESA in the KPPP mode. The derived time series of receiver clock offsets is used for assessing the receiver clock stability.

Second, collecting kinematic GPS daily data (with 10-s intervals) on 25 February 2015 of GRACE-A satellite equipped with ultrastable oscillator (USO) from German Research Centre for Geosciences (GFZ), the precise low Earth orbit (LEO) determination is performed using the standard PPP in order to obtain the time series of space-borne receiver clock offsets.

Finally, according to equation (2), the modified Allan variance is employed to evaluate the time series of various receiver clock offsets. In terms of the modified Allan deviations associated with the averaging time, Figure 2 shows the frequency stability for different types of oscillators including active hydrogen maser (H-maser), USO, cesium atomic clock (Cs), rubidium gas-cell oscillator (Rb), and temperature-compensated quartz crystal oscillator (TCXO), respectively. The receiver noises for the IF carrier phase and pseudorange observations are indicated by the dashed lines. The observation noise is usually assumed as white noise in the GNSS processing. In Figure 2, the GPS phase and code clock boundary is obtained using the undifferenced (UD) IF combined carrier phase and pseudorange observation residuals derived from PPP, respectively. As shown in formula (1), after the modeling of observations, the UD IF observation residuals (ε) contain several effects (e.g., multipath, and receiver tracking noise) that cannot be precisely modeled. Based on these UD observation residuals for single-receiver PPP, it is possible to derive the slope of the GPS phase noise boundary, which is different from the ideal slope (-1.5) in the case of using between-receiver single differenced observations (Weinbach, 2013).

In our PPP processing, the sampling interval of data is fixed (e.g., 1 s) so that we only need to focus on the modified Allan deviation at different averaging time for the given sampling interval. The modified Allan deviation for H-masers is within 1×10^{-11} if the averaging time is fixed to 30 s, while the deviation for TCXO with low clock quality is close to 1×10^{-10}. In fact, the quality of TXCO clocks cannot meet the requirement of PPP with receiver clock modeling. In contrast, the H-maser clocks with higher-frequency stability are

Figure 3. Positioning errors of kinematic PPP during the seismic quiet period.

qualified for the receiver clock modeling at the precision level of carrier phase. In addition, the reference clock modeling interval can be initially selected as the maximum averaging time for which the corresponding modified Allan deviation is below or close to the receiver noise boundary of the UD IF carrier phase observation residuals depicted as a dashed black line. For instance, the reference clock modeling intervals for USO and H-maser are set to around 2 min and 1 hr, respectively, which are circled in red in Figure 2. For each station involved for the receiver clock modeling, the modified Allan deviation is employed to evaluate the time series of receiver clock offsets derived from PPP and select the reference clock modeling interval for the subsequent PPP with receiver clock modeling. As shown in Figure 2, the Cs clock equipped by IGS station DAEJ can meet the requirement for receiver clock modeling. Besides, both Rb and commercial TCXO receiver clocks are not qualified for receiver clock modeling due to the limited frequency stability. In this case, the Rb and TCXO receiver clock offsets are also influenced by clock steering that synchronizes the receiver clock time and GPS time.

4. Analysis of PPP Performance

Based on the frequency stability analyses and numerous PPP results, the IGS tracking stations equipped with highly stable receiver clocks can be selected for the PPP solution with receiver clock modeling. In this study, PPP with receiver clock modeling is developed based on the iPPP software (Li, Zhang, et al., 2015).

To evaluate and compare the PPP performances, 1-Hz GNSS data are collected from station MGUE (equipped with the H-maser receiver clock) during the seismic quiet period and processed in the modes of GPS-only PPP with the modeling of receiver clock, GPS/GLONASS PPP with the modeling of receiver clock, and GPS/GLONASS standard PPP, respectively.

Figure 3 shows the PPP results of station MGUE in the kinematic mode comparing with the IGS reference station coordinates that have an accuracy of few millimeters. We can clearly see that the positioning accuracy in the horizontal components is better than that in the up component for GPS/GLONASS standard PPP. Because of receiver clock modeling, the improvement of the vertical positioning performance is particularly pronounced, which will make it possible to detect weak signals masked by high noise of the height estimates in the standard PPP approach.

As shown in Figure 3, a much shorter convergence time and a higher positioning accuracy can be obtained in the north, east, and up components with introducing GLONASS observations compared to
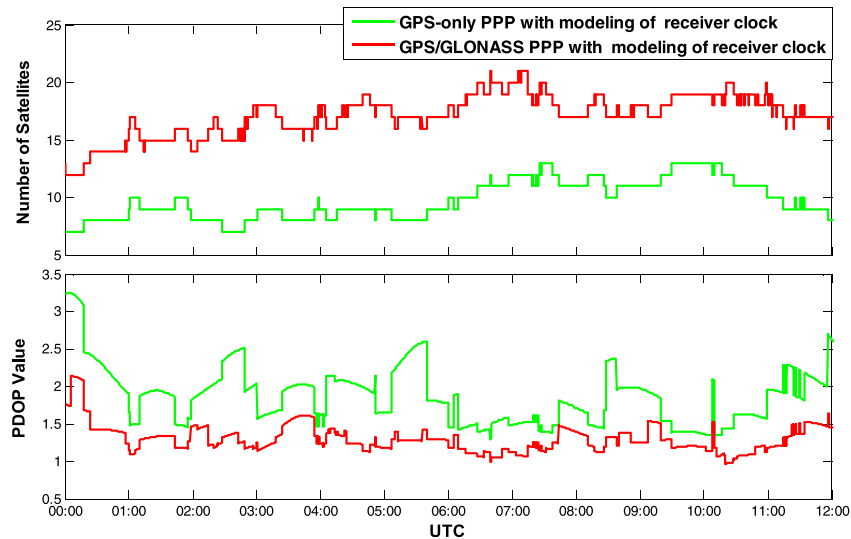
Figure 4. Comparisons of the PDOP values and available satellite numbers in GPS-only and GPS/GLONASS PPP solutions at station MGUE during the seismic quiet period.

GPS-only PPP with the modeling of receiver clock. For comparison, Figure 4 provides the number of available satellites and position dilution of precision (PDOP) values in the GPS/GLONASS combined and GPS-only cases. As for GPS-only PPP, about 7–13 satellites can be used at every epoch and the PDOP values range from 1.40 to 3.25. In contrast, the available satellite numbers for GPS/GLONASS PPP vary from 12 to 21 and the corresponding PDOP values are almost stable about 1.4. This confirms the increase of GLONASS enhances the spatial satellite geometry and thus improves the accuracy, convergence, and reliability of KPPP.

To further verify the superiority of GPS/GLONASS PPP with the modeling of receiver clock, the averaged root-mean-squares (RMSs) and standard deviations (STDs) of positioning errors are illustrated in Figure 5 based on the PPP results of station MGUE over a period of 1 month prior to the coastal Chile earthquake on 16 September 2015.

From Figure 5, it is obvious that GPS/GLONASS PPP with modeling of receiver clock is the best among the three solutions and its positioning accuracy in the north and east components are equivalent to that of GPS/GLONASS standard PPP. For GPS/GLONASS PPP with modeling of receiver clock, the STD and RMS values in the up component are respectively 17.5 and 24.4 mm, and the corresponding improvement in STD and RMS can reach up to 43.7% and 38.5% compared to GPS/GLONASS standard PPP. It is worthwhile to notice that the positioning accuracy in the north, east, and up components can be improved by about 30.3%, 26.5%, and 17.8%, respectively, due to the increase of GLONASS observations compared to GPS-only PPP with the modeling of receiver clock. With the development of new satellite systems, such as BDS, Galileo, and QZSS, there is a potential to perform the application of multi-GNSS PPP with receiver clock modeling.

For evaluation of the high-rate KPPP performance over a short period of time, the short-term STD values over the interval of 2 min in the north, east, and up components are summarized in Table 2 for the three different PPP solutions. In the case of GPS/GLONASS PPP with modeling of receiver clock, the averaged STD values are 3.5, 2.9, and 3.0 mm in the north, east, and up components, respectively. With receiver clock modeling, the short-term accuracy in the up component is about 2–4 mm, which usually cannot be obtained by the standard PPP. The short-term averaged STD values in the vertical direction can be improved by approximately 60% due to clock modeling comparing with the standard GPS/GLONASS PPP case. Owing to the addition of GLONASS, the improvement of short-term PPP accuracy can reach about 16.7%, 23.7%, and 18.9% in the north, east, and up components, respectively, compared to GPS-only PPP with modeling of receiver clock. The results clearly confirm that the short-term performance for GPS/GLONASS PPP with modeling of receiver clock is better than the other two solutions.
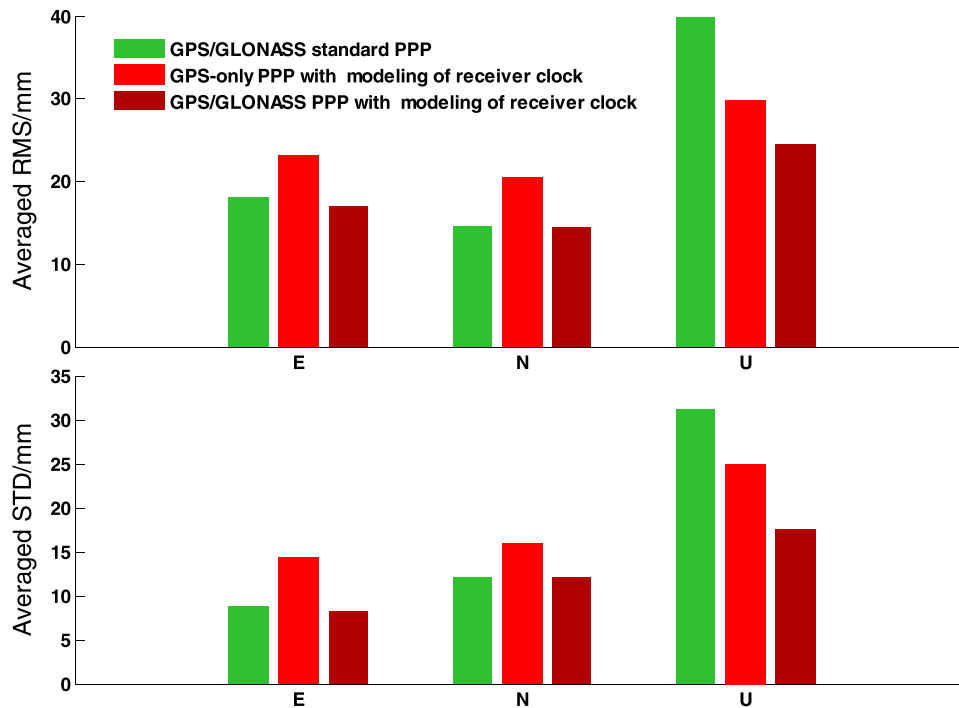
Figure 5. Averaged STD and RMS values in the north, east, and up components for different kinematic PPP solutions over a period of 1 month prior to the coastal Chile earthquake on 16 September 2015.

5. Seismic Displacement Monitoring

With the development of GNSS seismology, high-rate PPP has been successfully applied in measuring the seismic waveform (Ge et al., 2000; Kouba, 2003; Larson, 2009). Nevertheless, the PPP accuracy of seismic displacements in the vertical direction is usually compromised by huge noise of height estimates resulting from their high correlation with receiver clock offsets (Kouba, 2005). With receiver clock modeling, there is a great potential for achieving higher position accuracy and thus detecting more accurate seismic waves.

In this study, we take the Tohoku earthquake in 2011 and the Chile earthquakes in 2010 and 2015 as application examples of the seismic displacement monitoring. Based on clock and orbit products provided by ESA, 1-Hz high-rate GNSS data at IGS stations connected to the highly stable receiver clocks are processed in the solutions of GPS-only and GPS/GLONASS PPP with receiver clock modeling.

5.1. Tohoku Earthquake: GPS-Only PPP With Modeling of Receiver Clock

The magnitude 9.0 Tohoku earthquake occurred near the northeast area of Honshu in Japan, on 11 March 2011 (Lay & Kanamori, 2011). The IGS network of tracking ground stations in Japan has contributed to a good understanding of the rupture physics for the massive earthquake. Several receiver clocks of the GPS stations in the network are qualified for receiver clock modeling. In order to analyze the impact of receiver clock modeling on seismic displacement monitoring, 1-Hz GPS data from the IGS stations SHAO, DAEJ, and USUD are processed through GPS-only KPPP. As shown in Figure 6, the three IGS stations are located around 1,888, 1,342, and 429 km, respectively, from the earthquake epicenter (142.372°E, 38.297°N), which occurred at 05:46:24 UTC at 30-km depth.
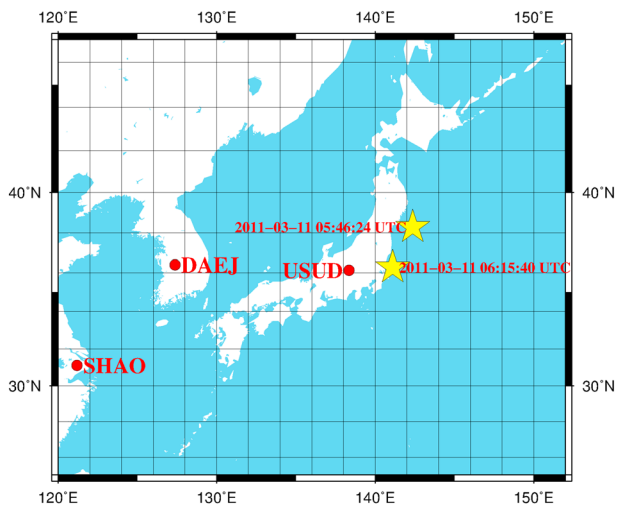
Table 2
Averaged STD Values Over 2 min in the North, East, and Up Components for Different Kinematic PPP Solutions Over the Period Between 15 July 2015 and 16 September 2015

Time period(UTC)	GPS/GLONASS PPP with receiver clock modeling (mm)			GPS/GLONASS PPP without receiver clock modeling (mm)			GPS-only PPP with receiver clock modeling (mm)		
	E	N	U	E	N	U	E	N	U
02:00:00–02:02:00	3.9	3.7	2.2	3.8	3.5	7.1	4.9	4.5	2.8
03:00:00–03:02:00	3.5	4.6	2.0	3.6	5.1	8.5	3.7	5.8	2.3
04:00:00–04:02:00	1.6	2.0	3.1	1.8	2.2	7.5	2.4	2.5	3.7
05:00:00–05:02:00	2.5	4.5	3.6	2.7	4.8	8.0	3.8	5.5	3.9
06:00:00–06:02:00	4.5	2.2	4.4	4.7	2.3	7.8	5.6	3.0	5.7
07:00:00–07:02:00	3.0	4.0	2.9	3.0	3.9	7.3	4.0	4.6	4.2
08:00:00–08:02:00	2.7	3.5	2.9	3.3	4.0	7.4	3.5	4.2	3.2
09:00:00–09:02:00	1.5	3.2	3.0	2.0	3.5	6.9	2.2	3.3	3.5
Average	2.9	3.5	3.0	3.1	3.7	7.5	3.8	4.2	3.7

Figure 6. Distribution of the epicenters of the 2011 Tohoku earthquake depicted as yellow pentagram and GPS tracking stations SHAO (equipped with H-maser clock), DAEJ (equipped with Cs clock), and USUD (equipped with H-maser clock).

Figure 7 shows the KPPP positioning results of IGS stations (namely, SHAO and DAEJ) with respect to IGS published station coordinates (before the earthquake) that commonly have an accuracy of few millimeters (Dow et al., 2009) during the main shock. Additionally, the static 1-Hz GPS data before and after the earthquake are collected and then processed by KPPP with or without receiver clock modeling for all the IGS tracking stations (SHAO, DAEJ, CONZ, USUD, and MGUE). Similar to those in section 4, the results show that the vertical accuracy of PPP can be improved by 30–40% in terms of RMS due to receiver clock modeling, while the improvement in the horizontal directions is very slight.

From the IGS published station coordinates before and after earthquake, we calculate the offsets of station SHAO caused by the earthquake that are about 0.1, 5.7, and 3.1 mm in the east, north, and up components, respectively. However, in the case of standard PPP, the offsets of about 18 cm in the up component and about 2 cm in the north component after 06:00:00 UTC are not reliable. With the modeling of receiver clock, the significant improvement of the vertical seismic displacement ranges from 5 cm to 18 cm before and after earthquake, while the horizontal variations are relatively small (less than 2.0 and 1.2 cm in the north and east components, respectively). This is reasonable due to the fact that the receiver clock offsets have a high correlation with the height position estimates at every observation epoch compared to the low correlation with horizontal position estimates. With receiver clock modeling, a high degree of decoupling between height position estimates and receiver clock offsets can be achieved.

Figure 8 provides correlation coefficients between height position and receiver clock estimates at each epoch during the main shock. The mean correlation coefficients of the three IGS stations are depicted in the column graph below for comparisons. It can be seen that there is an obvious periodicity exhibited in the plots of the correlation coefficients. This results from the linear interpolation of clock errors for precise satellite clock products with a sampling rate of 30 s. However, the periodicity is not obvious when the precise satellite clock products with higher sampling interval (e.g., 5 s) are used. As shown in Figure 8, the correlations are reduced by a factor of 1.49 (for station DAEJ with 15 min of modeling interval) to 26.71
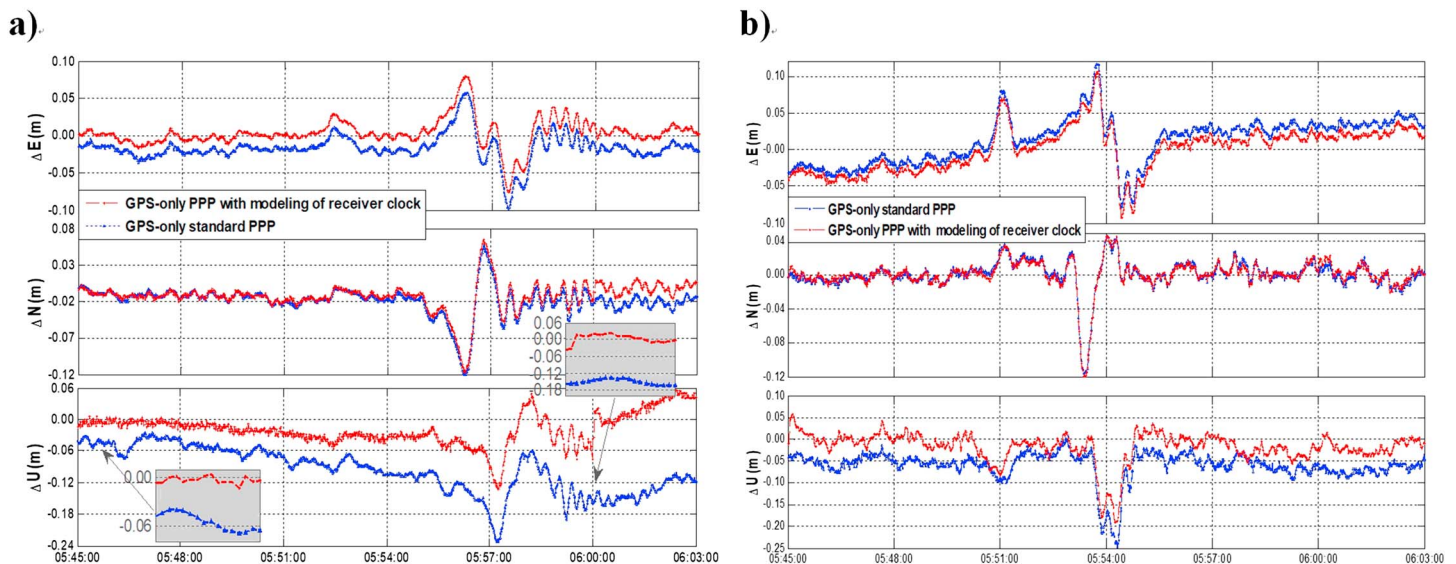

Figure 7. Kinematic GPS-only PPP position solutions during the 9.0 magnitude main shock for the massive Tohoku earthquake on 11 March 2011. (a) For station SHAO equipped with the H-maser clock and (b) for station DAEJ equipped with the Cs clock.
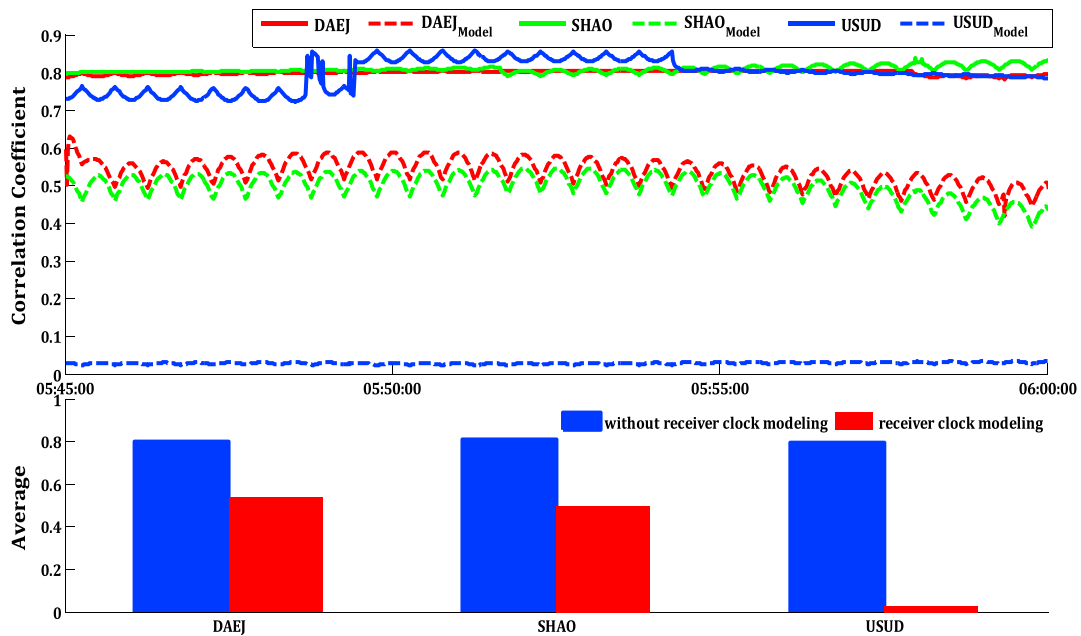
Figure 8. Correlation coefficients between the height position estimates and receiver clock offsets for the IGS stations DAEJ, SHAO, and USUD during the 9.0 magnitude main shock for the massive Tohoku earthquake on 11 March 2011 and the averaged correlation coefficients for the stations during the period.

(for station USUD with 2 hr of modeling interval) due to receiver clock modeling. With the increase of clock modeling interval, a higher degree of decoupling can be achieved.

In the case of 30 s of GPS data sampling rate, Cs clock does not meet the requirement for receiver clock modeling (Wang et al., 2015). In contrast, the 1-Hz data can significantly reduce the process noise in the
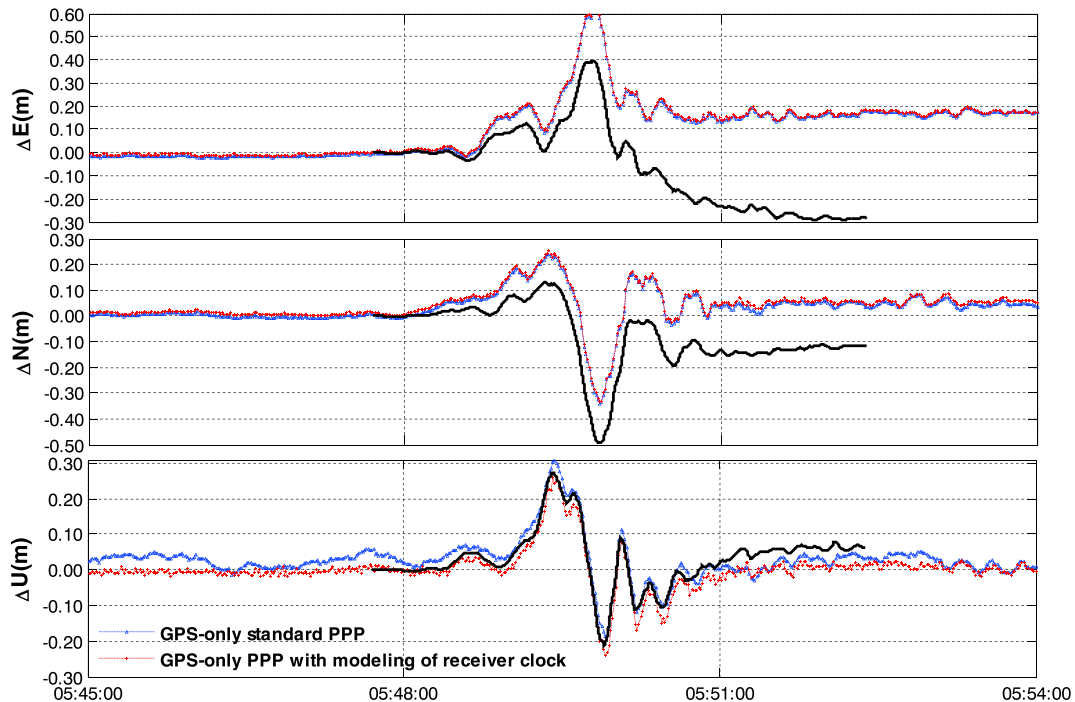

Figure 9. Comparisons of the seismic-only displacement waveforms at the seismic station NGN014 and PPP-based seismic displacement waveforms with and without receiver clock modeling at the IGS station USUD equipped with H-maser clock during the 9.0 magnitude main shock for the massive Tohoku earthquake on 11 March 2011. The seismic displacement waveforms integrated from acceleration data are shown by the black line.
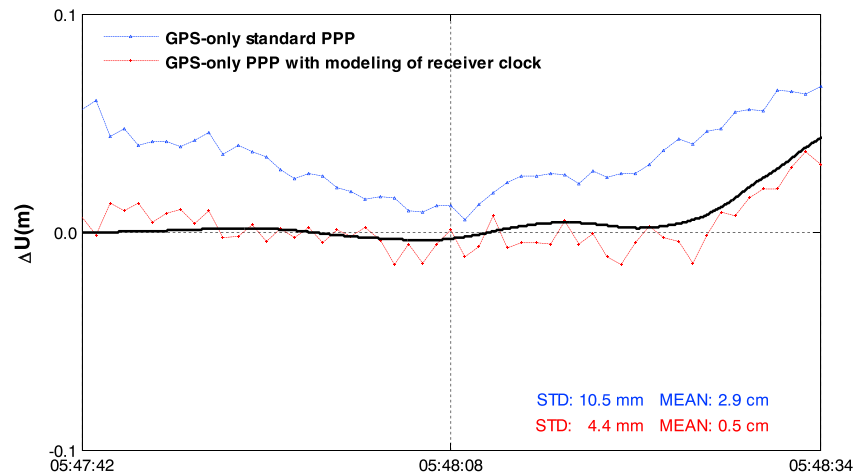
Figure 10. Comparisons of the vertical seismic-only displacement waveforms at the seismic station NGN014 and displacement waveforms derived from PPP with or without receiver clock modeling at IGS station USUD (equipped with H-maser clock) over a short period for the main shock of the 9.0 magnitude massive Tohoku earthquake on 11 March 2011. The seismic displacement waveforms integrated from acceleration data are shown by the black line.

Kalman filter. From Figure 7, the receiver clock modeling for 1-Hz GPS data shows a certain improvement in the vertical direction at station DAEJ equipped with Cs clock. Similarly, the improvement of the vertical seismic displacement can reach around 5 cm due to receiver clock modeling, while the horizontal displacements rarely vary.

The seismic station NGN014 from the Kiban Kyoshin network (Kik-net) operated by National Research Institute for Earth Science and Disaster Resilience is colocated with the IGS tracking station USUD (about 11.6-km distance). Based on the strong motion data with 100-Hz sampling rate at station NGN014 for the 2011 Tohoku earthquake, the corresponding seismic-only waveform are derived from double integration of acceleration data after the baseline correction, which is a bilinear least squares fit over full record (Guo, 2015; Guo et al., 2014; Wang et al., 2011). Figure 9 shows the seismic-only and PPP-based displacement waveforms at the stations NGN014 and USUD, respectively. The PPP-based displacement waveforms of station USUD show a high degree of resemblance relative to those integrated from the acceleration data at the colocated seismic station NGN014. During the main shock, strong movements of the seismic instrument can lead to the baseline offsets and distortions, so a permanent coseismic offset is lost in the seismic-only waveform in the up, east, and north components. We can also see that the PPP-based horizontal waveforms are slightly affected by receiver clock modeling, while the vertical component shows an obvious change.

As shown in Table 2, the improvement in the short-term accuracy of PPP in the vertical direction is considerable due to receiver clock modeling. For investigating the impact of the clock modeling on the short-term PPP accuracy to measure the vertical seismic wave motions, Figure 10 presents the vertical seismic displacement waveforms at the stations NGN014 and USUD over the period from UTC 05:47:42 to UTC 05:48:34. For the standard PPP, the vertical seismic waveform is masked by huge noise as expected. However, the vertical noise is significantly reduced due to receiver clock modeling and thus the improved PPP-based seismic waveform in the vertical component matches very well with that integrated from the acceleration data. Compared to the standard PPP, the averaged offset of about 2.4 cm from the external seismic-only displacements over the short period can be corrected by receiver clock modeling. The short-term STD value for differences between the standard GPS-only PPP displacements and the displacements integrated from accelerometers is 10.5 mm. With receiver clock modeling, the short-term accuracy of GPS-only PPP seismic displacements is 4.4 mm and improved by about 58.0% compared to that for the standard PPP.

On 11 March 2011 at 06:15:40 UTC, near the east coast of Honshu, Japan, a 7.9 magnitude aftershock occurred with an epicenter (141.111°E, 36.281°N) at 42-km depth. Figure 11 shows seismic displacements of station USUD during the 7.9 magnitude earthquake. From Figure 11, it can be seen that the vertical accumulated errors of seismic displacement can be eliminated due to receiver clock modeling, while the undesirable low-amplitude noise with short wavelength is introduced into vertical seismic displacements. This indicates that the process noise matrix in the Kalman filter is not well controlled when the receiver clock offset estimate
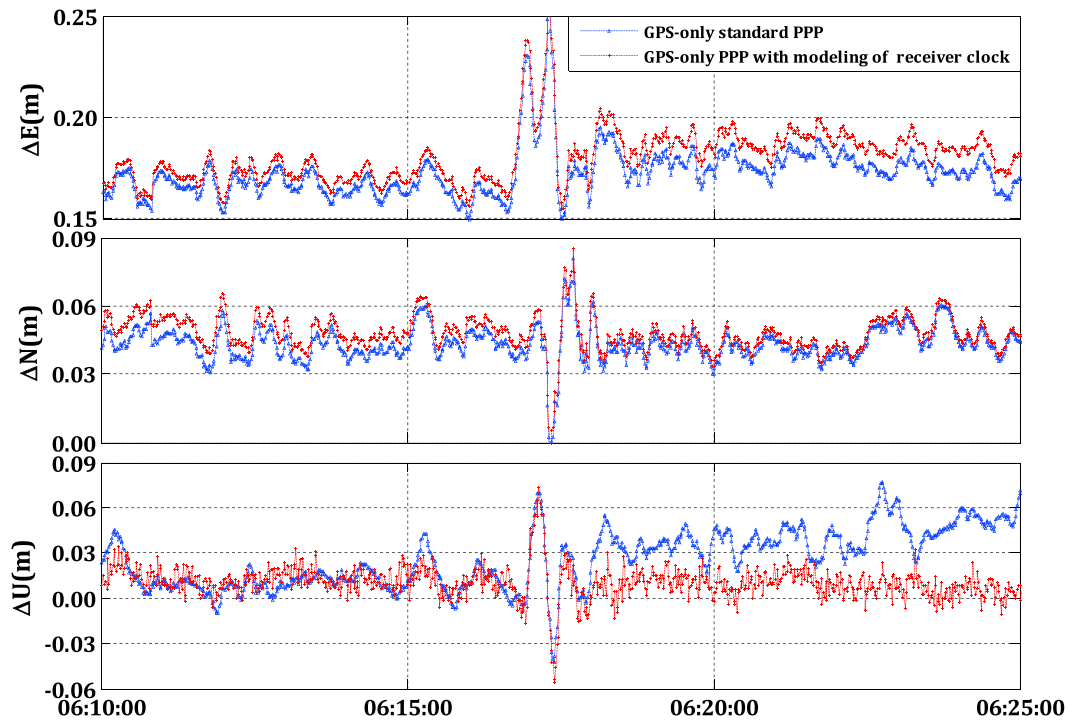
Figure 11. PPP-based seismic displacements at station USUD during the 7.9 magnitude Tohoku aftershock on 11 March 2011.

is constrained by the receiver clock modeling over 1-hr modeling interval according to its known stability. Although some sort of undesirable noise are introduced into vertical seismic displacements, the positioning accuracy in the vertical direction before and after the earthquake is still improved due to receiver clock modeling compared to the standard PPP solution.

5.2. Chile Earthquakes: GPS/GLONASS PPP With Modeling of Receiver Clock

All the above tests focus on GPS-only PPP with receiver clock modeling, whereas the advantage of receiver clock modeling in seismic displacement monitoring should be linked to the more robust GPS/GLONASS combined PPP processing. Thus, we take the Chile earthquakes as an example to demonstrate the feasibility of monitoring seismic displacement through GPS/GLONASS PPP with the receiver clock modeling.

The M_w 8.8 Maule, Chile, earthquake occurred near the boundary between the South American and Nazca Plates, on 27 February 2010. The selected IGS station CONZ was equipped with a well-maintained H-maser oscillator and located about 100 km from the epicenter for the main shock, as shown in Figure 12. For comparison, 1-Hz high-rate GNSS data of station CONZ during the earthquake are processed by using GPS/GLONASS PPP with and without receiver clock modeling.

The station CONZ is colocated with the seismic station CCSP (about 7.8-km distance) operated by the University of Chile. The seismic-only waveforms are obtained by the double integration of acceleration data after the baseline correction based on the 100-Hz strong motion data at station CCSP for the 2010 Chile earthquake. Figure 13 shows the dynamic seismic displacements in east, north, and up
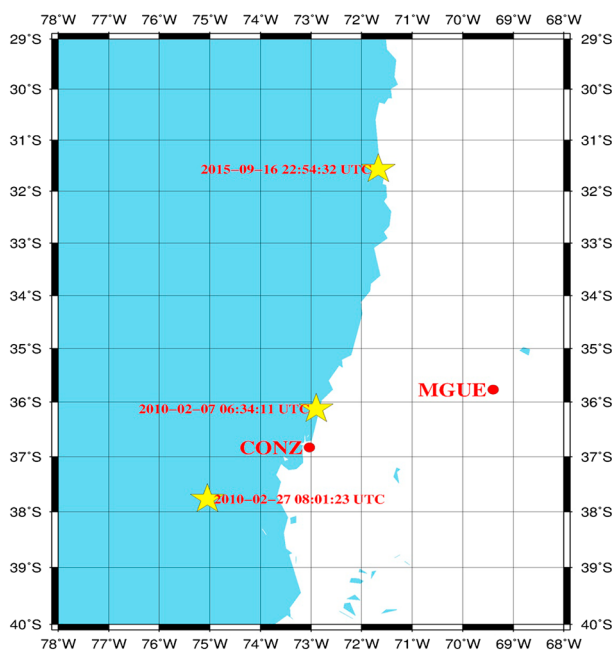

Figure 12. Distribution of the epicenters of the 2010 and 2015 Chili earthquakes depicted as yellow pentagram and GPS/GLONASS tracking stations MGUE (equipped with H-maser clock) and CONZ (equipped with H-maser clock).
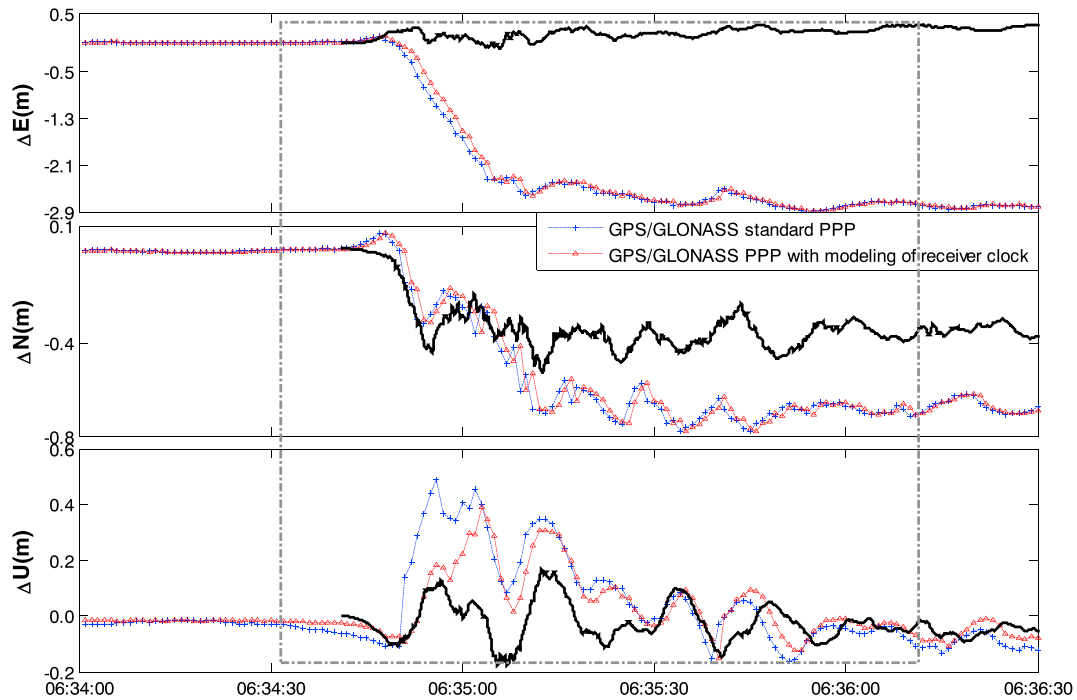
Figure 13. Comparisons of the seismic-only displacement waveforms at the seismic station CCSP and displacement waveforms derived from PPP with or without receiver clock modeling at IGS station CONZ equipped with H-maser clock during the main shock of the 8.8 magnitude Maule earthquake on 27 February 2010. The seismic displacement waveforms integrated from acceleration data are shown by the black line.

components for GPS/GLONASS PPP without or with the clock modeling with 30-min modeling interval and the seismic-only displacements from accelerometers for comparison. From Figure 13, we can clearly see that the seismic-only waveforms from accelerometers show obvious permanent coseismic offsets in the three components, similar to the GPS-only case shown in Figure 9. However, the seismic waveforms integrated from acceleration data can be considered as relatively reliable during the short-term period of initial seismic deformation since the movement of seismic instruments is not significant at this stage. Additionally, the results have confirmed that the vertical GPS/GLONASS PPP accuracy can be improved due to receiver clock modeling in section 4. Thus, we further investigate its impact on GPS/GLONASS PPP accuracy to detect the vertical seismic wave motion over the short-term initial period.
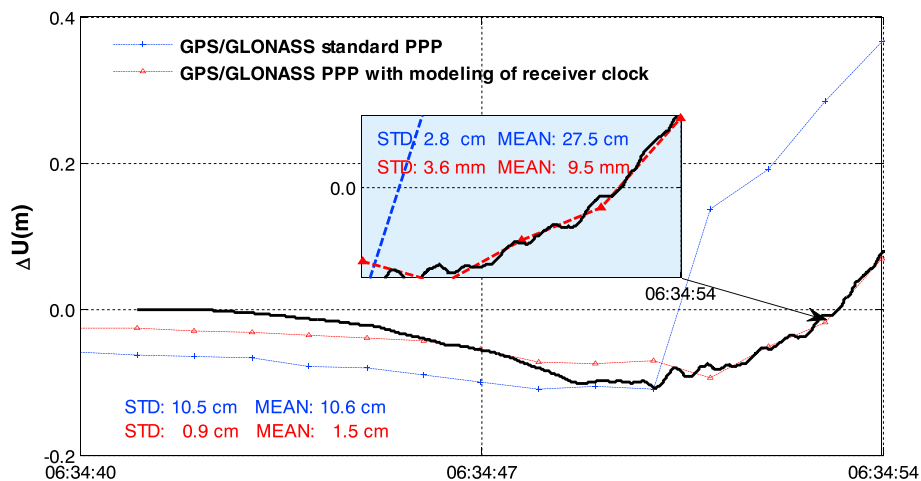

Figure 14. Comparisons of the seismic-only displacement waveforms at the seismic station CCSP and displacement waveforms derived from PPP with and without receiver clock modeling at IGS station CONZ (equipped with H-maser clock) over a short period for the main shock of the 8.8 magnitude Maule earthquake on 27 February 2010. The seismic displacement waveforms integrated from acceleration data are shown by the black line.
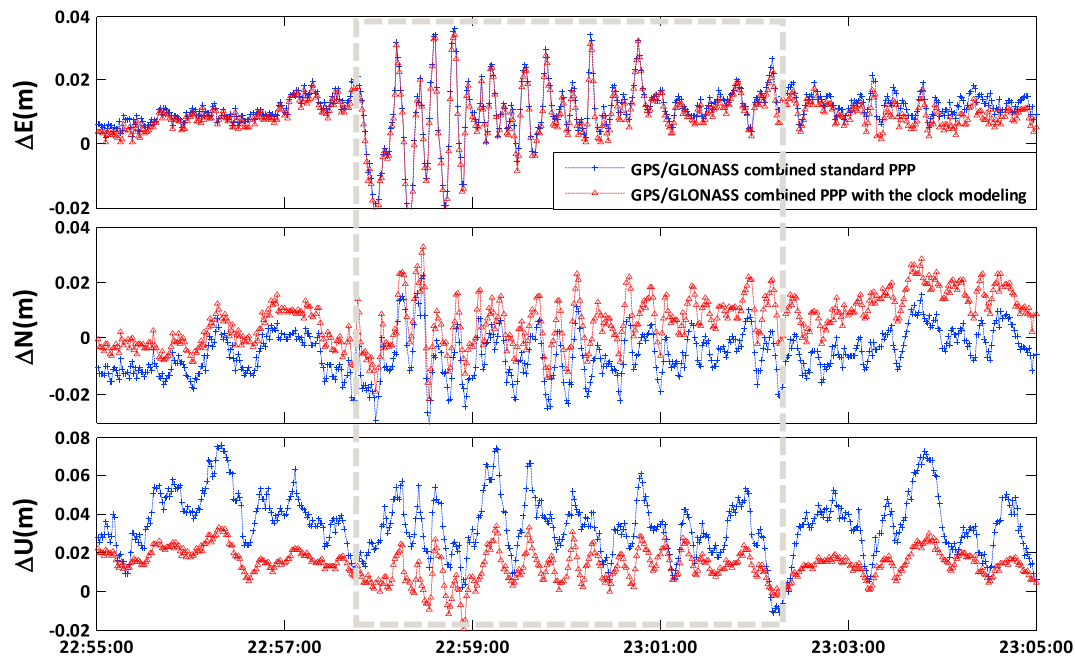
Figure 15. Kinematic GPS/GLONASS PPP position solution at station MGUE for the shock of the magnitude 8.3 coastal Chile earthquake on 16 September 2015.

Figure 14 shows the vertical seismic displacement waveforms at the stations CCSP and CONZ during the initial seismic period from UTC 06:34:40 to UTC 06:34:54. From Figure 14, we can see that the vertical seismic waveform derived from GPS/GLONASS PPP with receiver clock modeling shows a better agreement with that integrated from acceleration data than the GPS/GLONASS standard PPP case. The results show that receiver clock modeling can correct an averaged offset of about 9.0 cm from the external seismic-only displacements over the initial period. The STD value for differences between the standard GPS/GLONASS PPP displacements and the displacements integrated from accelerometers over the period is 10.5 cm. Because of receiver clock modeling, the accuracy of GPS/GLONASS PPP dynamic seismic displacements can be improved to the level of up to 9 mm. In fact, the observation environment over the short period is very poor with a limited number of satellites available for monitoring the initial active seismic deformation. For instance, only three GPS satellites were available during the period from 06:34:50 UTC to 06:34:54 UTC. Consequently, the results of GPS-only PPP are not continuous and reliable in this case. As shown in Figure 14, the PPP seismic waveform can be bridged by using the additional GLONASS data over the span of time. Taking the vertical seismic-only waveform derived from accelerometers as reference, the STD values for the standard GPS/GLONASS PPP and improved GPS/GLONASS PPP displacement differences are 2.8 cm and 3.6 mm, respectively, under such poor observational condition. The results confirm that the short-term accuracy of better than 4 mm for GPS/GLONASS PPP vertical seismic displacements is achievable due to the receiver clock modeling. For IGS station CONZ, the short-term accuracy in the vertical direction can be improved by a factor of 7 due to receiver clock modeling compared to the GPS/GLONASS standard PPP in the case of the 8.8 magnitude Maule earthquake on 27 February 2010.

On 16 September 2015 at 22:54:32 UTC, the magnitude 8.3 Chile earthquakes occurred near the west area of Illapel, resulting from the thrust faulting on the interface zone between South America and Nazca Plates. In order to further analyze the coastal Chile earthquake, 1-Hz high-rate GNSS data of station MGUE about 513 km away from the epicenter are processed by using GPS/GLONASS PPP with and without the clock modeling. Figure 15 shows seismic displacements relative to the IGS published coordinates of station MGUE during the main shock period. Compared to the vertical frequent fluctuations for the standard PPP, the time series of vertical seismic displacements before and after the main shock is more stable with only millimeter-level amplitude and thus the variations of vertical seismic displacements during the main shock (in the gray dashed box) can be detected due to receiver clock modeling.

6. Conclusions

In this study, the GPS/GLONASS combined PPP with the modeling of highly stable receiver clock is applied to the active seismic deformation monitoring for the first time. The comparative results show that with the increase of GLONASS observations, the long-term positioning accuracy in the north, east, and up components can be improved by about 30.3%, 26.5%, and 17.8%, respectively, compared to GPS-only PPP with the modeling of receiver clock. Because of receiver clock modeling, the short-term PPP accuracy of 2–4 mm is achievable in the vertical component, which usually cannot be obtained in the standard PPP solution. As the potential correlation among the receiver clock estimates over a short time period is considered for the clock modeling, a higher degree of decorrelation between the height position estimates and receiver clock offsets can be achieved compared to the standard PPP case. Subsequently, the accuracy of the PPP-derived vertical seismic displacements can be enhanced. Results show that the proper modeling of highly stable receiver clocks considerably reduces huge noise of vertical seismic displacement so that the weak seismic signatures in vertical direction can be detected.

In summary, based on high-rate GNSS data of IGS stations during the 2011 Japan and 2010 and 2015 Chile earthquakes, it has been demonstrated that GNSS seismology could benefit from the receiver clock modeling. Taking the external seismic-only waveform derived from accelerometers as reference, we further analyze the impact of the clock modeling on PPP accuracy to monitor active seismic deformation. The short-term GPS-only PPP accuracy to detect seismic wave motion in the vertical direction is improved by about 58% to 4.4 mm due to the modeling of highly stable receiver clocks. For GPS/GLONASS combined PPP seismic displacements in the vertical direction, the short-term accuracy can be improved to 4 mm because of the receiver clock modeling.

Along with the densification of the global network of GNSS ground stations connected to highly stable atomic clocks and the development of GNSS systems (i.e., GPS, GLONASS, Galileo, BDS, QZSS, and so on), multi-GNSS PPP with the receiver clock modeling would be widely used for a great variety of global scientific applications, for example, GNSS seismology as presented in this study.

References

Böhm, J., Möller, G., Pain, G., Schindelegger, M., & Weber, R. (2015). Development of an improved empirical model for slant delays in the troposphere (GPT2w). *GPS Solutions*, 19(3), 433–441. https://doi.org/10.1007/s10291-014-0403-7

Boore, D. M., Stephens, C. D., & Joyner, W. B. (2002). Comments on baseline correction of digital strong-motion data: Examples from the 1999 Hector Mine, California, earthquake. *Bulletin of the Seismological Society of America*, 92(4), 1543–1560. https://doi.org/10.1785/0120000926

Brown, R. G., & Hwang, P. Y. C. (Eds) (2005). *Introduction to random signals and applied Kalman filtering* (3rd ed.). New York: John Wiley.

Cai, C., & Gao, Y. (2013). Modeling and assessment of combined GPS/GLONASS Precise Point Positioning. *GPS Solutions*, 17(2), 223–236. https://doi.org/10.1007/s10291-012-0273-9

Dierendonck, A. J., McGraw, J. B., & Brown, R. G. (1984). Relationship between Allan variances and Kalman filter parameters. In Processing of the 16th Annual Precise Time and Time Interval (PTTI) Applications and Planning Meeting. Greenbelt, MD, 27–29, Nov, 1984.

Dow, J. M., Neilan, R. E., & Rizos, C. (2009). The international GNSS service in a changing landscape of Global Navigation Satellite Systems. *Journal of Geodesy*, 83(3-4), 191–198. https://doi.org/10.1007/s00190-008-0300-3

Ge, L., Han, S., Rizos, C., Ishikawa, Y., Hoshiba, M., Yoshida, Y., et al. (2000). GPS seismometer with up to 20-Hz sampling rate. *Earth, Planets and Space*, 52(10), 881–884. https://doi.org/10.1186/BF03352300

Ge, M., Gendt, G., Rothacher, M., Shi, C., & Liu, J. (2008). Resolution of GPS carrier-phase ambiguities in Precise Point Positioning with daily observations. *Journal of Geodesy*, 82(7), 389–399. https://doi.org/10.1007/s00190-007-0187-4

Guo B. (2015). Methods of coseismic displacement estimation using a single high-rate GNSS receiver and combining with strong-motion seismometers for earthquake early warning (in Chinese), (Doctoral dissertation), Retrieved from CNKI (http://www.cnki.net/KCMS/detail/), MI: Wuhan University.

Guo, B., Zhang, X., & Li, X. (2014). Integration of GNSS and seismic data for earthquake early warning: A case study on the 2011 M_w 9.0 Tohoku-Oki earthquake. In *China Satellite Navigation Conference (CSNC) 2014 Proceedings* (Rep. 2, Vol. 2, pp. 437–450). Berlin: Springer.

Herring, T. A., Davis, J. L., & Shapiro, I. I. (1990). Geodesy by radio interferometry: The application of Kalman filtering to the analysis of very long baseline interferometry data. *Journal of Geophysical Research*, 95(B8), 12,561–12,581. https://doi.org/10.1029/JB095iB08p12561

Hirahara, K., Nakano, T., Hoso, Y., Matsuo, S., & Obana, K. (1994). An experiment for GPS strain seismometer. In *Japanese Symposium on GPS*, (Rep., pp. 67–75), Tokyo, Japan, 15–16 December.

Kouba, J. (2003). Measuring seismic waves induced by large earthquake with GPS. *Studia Geophysica et Geodaetica*, 47(4), 741–755. https://doi.org/10.1023/A:1026390618355

Kouba, J. (2005). A possible detection of the 26 December 2004 great Sumatra-Andaman islands earthquake with solution products of the International GNSS Service. *Studia Geophysica et Geodaetica*, 49(4), 463–483. https://doi.org/10.1007/s11200-005-0022-4

Kouba, J., & Héroux, P. (2001). Precise Point Positioning using IGS orbit and clock products. *GPS Solutions*, 5(2), 12–28. https://doi.org/10.1007/PL00012883

Larson, K. M. (2009). GPS seismology. *Journal of Geodesy*, 83(3-4), 227–233. https://doi.org/10.1007/s00190-008-0233-x

Lay, T., & Kanamori, H. (2011). Insights from the great 2011 Japan earthquake. *Physics Today*, 64(12), 33–39. https://doi.org/10.1063/PT.3.1361

Li, X., Ge, M., Dai, X., Ren, X., Fritsche, M., Wickert, J., & Schuh, H. (2015). Accuracy and reliability of multi-GNSS real-time precise positioning: GPS, GLONASS, BeiDou, and Galileo. *Journal of Geodesy*, 89(6), 607–635. https://doi.org/10.1007/s00190-015-0802-8

Li, X., Ge, M., Zhang, H., & Wickert, J. (2013). A method for improving uncalibrated phase delay estimation and ambiguity-fixing in real-time Precise Point Positioning. *Journal of Geodesy*, 87(5), 405–416. https://doi.org/10.1007/s00190-013-0611-x

Li, X., Zhang, X., Ren, X., Fritsche, M., Wickert, J., & Schuh, H. (2015). Precise positioning with current multi-constellation Global Navigation Satellite Systems: GPS, GLONASS, Galileo and Beidou. *Scientific Reports*, 5(1). https://doi.org/10.1038/srep08328

Wang, F. H., Chen, X. H., & Guo, F. (2015). GPS/GLONASS combined Precise Point Positioning with receiver clock modeling. *Sensors*, 15(7), 15,478–15,493. https://doi.org/10.3390/s150715478

Wang, K., & Rothacher, M. (2013). Stochastic modeling of high-stability ground clocks in GPS analysis. *Journal of Geodesy*, 87(5), 427–437. https://doi.org/10.1007/s00190-013-0616-5

Wang, R., Schurr, B., Milkereit, C., Shao, Z., & Jin, M. (2011). An improved automatic scheme for empirical baseline correction of digital strong-motion records. *Bulletin of the Seismological Society of America*, 101(5), 2029–2044. https://doi.org/10.1785/0120110039

Weinbach, U. (2013). Feasibility and impact of receiver clock modeling in precise GPS data analysis (Doctoral Dissertation). MI: Gottfried Wilhelm Leibniz Universität Hannover.

Weinbach, U., & Schön, S. (2011). GNSS receiver clock modeling when using high-precision oscillators and its impact on PPP. *Advances in Space Research*, 47(2), 229–238. https://doi.org/10.1016/j.asr.2010.06.031

Weinbach, U., & Schön, S. (2013). Improved GRACE kinematic orbit determination using GPS receiver clock modeling. *GPS Solutions*, 17(4), 511–520. https://doi.org/10.1007/s10291-012-0297-1

Weinbach, U., & Schön, S. (2015). Improved GPS-based coseismic displacement monitoring using high-precision oscillators. *Geophysical Research Letters*, 42, 3773–3779. https://doi.org/10.1002/2015GL063632

Zhang, X., & Andersen, O. B. (2006). Surface ice flow velocity and tide retrieval of the Amery ice shelf using Precise Point Positioning. *Journal of Geodesy*, 80(4), 171–176. https://doi.org/10.1007/s00190-006-0062-8